Inorganic Chemistry

Article

pubs.acs.org/IC

Tetranuclear Gadolinium(III) Porphyrin Complex as a Theranostic Agent for Multimodal Imaging and Photodynamic Therapy

Jian Luo, Li-Feng Chen, Ping Hu, and Zhong-Ning Chen*

State Key Laboratory of Structural Chemistry, Fujian Institute of Research on the Structure of Matter, Chinese Academy of Sciences, 155 Yangqiao Road West, Fuzhou 350002, China

Supporting Information

ABSTRACT: We describe herein the elaborate design of a Gd(III)−porphyrin complex as a theranostic agent for multimodal imaging and photodynamic therapy. Far-red-emitting (665 nm) and high relaxivity (14.1 mM^{-1} s^{-1}) with 107% increase upon binding to HSA (human serum albumin) (29.2 mM^{-1} s^{-1}) together with efficiently generating singlet oxygen upon exposure to far-red light irradiation at 650 ± 20 nm demonstrate that this Gd(III)−porphyrin complex with four Gd(III)−DTTA units bound to tetraphenylporphyrin acts as a potentially theranostic agent with excellent performance for magnetic resonance imaging, optical imaging, and photodynamic therapy.

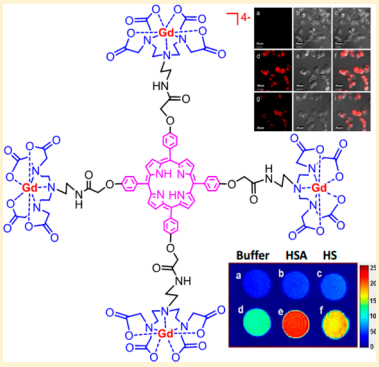

INTRODUCTION

Diagnosis and therapy are traditionally regarded as two separate issues in medical care. To get an optimal curative effect for many diseases, especially for cancer, they have been combined mutually and synergistically.[1,2] Theranostic agents provide a feasible approach to accurately locate the tumor tissues and monitor the therapeutic responses to individual treatments.[3] With the rapid development of nanomedicine, many theranostic agents based on nanomaterials have been reported,[3−7] although their physiological toxicity remains to be clarified. Nevertheless, most of the clinically used diagnostic and therapeutic drugs are organic or coordination compounds, in which their physiological action has been well understood. Therefore, development of metal-coordination or organometallic compounds as theranostic agents that combine both diagnostic and therapeutic functions is more appealing in clinical application.

Among multiple diagnostic imaging techniques, MRI (magnetic resonance imaging) as a noninvasive diagnosis mode can provide perfectly whole body images with excellent spatial and anatomical resolution.[8−12] Photodynamic therapy (PDT) is a clinically therapeutic modality using a photosensitizer (PS) and light irradiation to eradicate cancer tissues.[13−15] Upon irradiation with the proper wavelength of light, the PS interacts with molecular oxygen to generate cytotoxic singlet oxygen ($^1O_2$) for killing cancer cells. Furthermore, the inherent photoluminescence of the PS can also be used for fluorescence imaging to locate the disease, which is often referred to as photodynamic diagnosis (PDD).[3,16,17]

Gd(III)-based chelates are widely utilized as contrast agents of MRI in clinical diagnosis.[8−12,18−22] Porphyrins are clinically used in PDT for cancer treatments because of their capability to efficiently generate singlet oxygen and the tendency to preferentially accumulate in tumor tissue.[13−17] Considering that both functions of Gd(III)-based chelate in MRI and porphyrin in PDT are likely achieved in a combined compound, complex **6** (Scheme 1) is elaborately designed as a novel theranostic agent with much improved function relative to the individual precursors.

Scheme 1. Structure of Complex 6

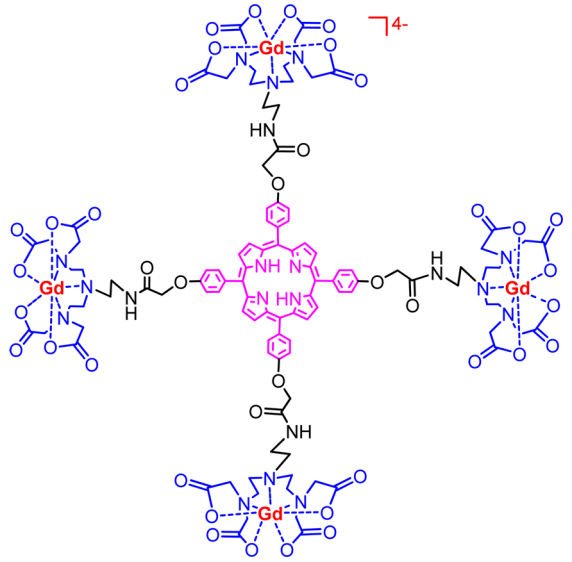

As shown in Scheme 1, four Gd(III)−DTTA chelate moieties are incorporated to tetraphenylporphyrin (TPP) through covalent

Received: January 29, 2014
Published: April 2, 2014

   dx.doi.org/10.1021/ic500238s | Inorg. Chem. 2014, 53, 4184−4191

Scheme 2. Synthetic Routes for $TPP(H_4DTTA)_4$[a]

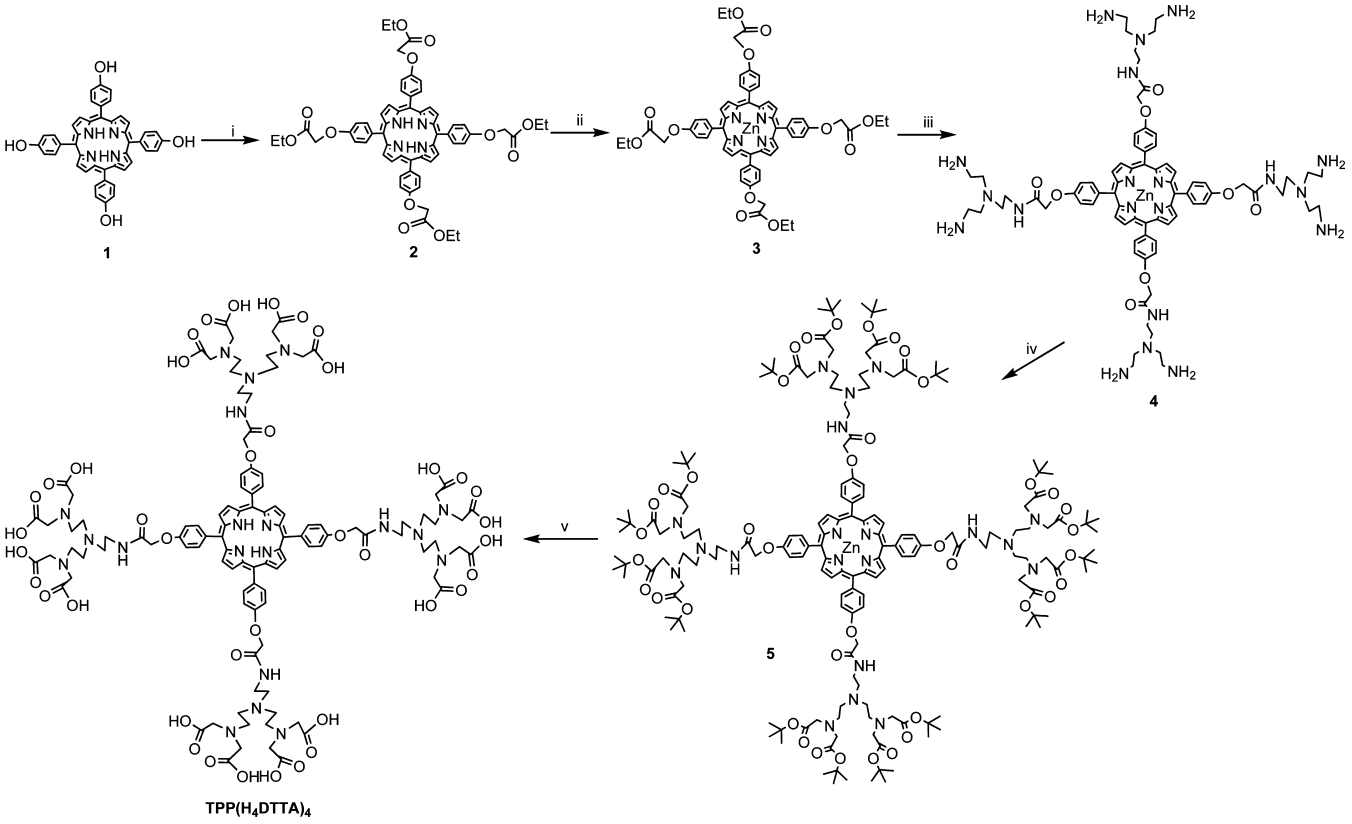

[a](i) Ethyl bromoacetate, K_2CO_3, 18-crown-6, room temperature for 1 day. (ii) $Zn(OAc)_2{\cdot}2H_2O$, refluxed for 4 h. (iii) Tris(2-aminoethyl)amine, refluxed for 2 days. (iv) Bromoacetic acid ethyl ester, $NaHCO_3$, 50 °C for 2 days. (v) Trifluoroacetic acid, room temperature for 1 day.

linkages. The chelating character of the DTTA moiety ensures thermodynamic stability, in vivo safety, and fast water exchange of complex **6**.[22] Attachment of four Gd–DTTA units to a rigid TPP moiety results in a much higher relaxivity (14.1 mM^{-1} s^{-1}) per Gd(III) than those of MRI contrast agents (3.0–6.0 mM^{-1} s^{-1}) in clinical diagnosis.[9,19] The four negative charge of complex **6** induces excellent water solubility and HSA (human serum albumin) binding character.[19,23] Upon binding to HSA, the relaxivity is remarkably enhanced from 14.1 to 29.2 mM^{-1} s^{-1}. Because of much better water solubility compared with free TPP, the capability of complex **6** to generate singlet oxygen is significantly improved upon irradiation with a far-red light (650 ± 20 nm). The superior far-red excitation (650 nm) and emission (665 nm) ensure complex **6** is applicable to PDT and PDD in deep tissue.[5,24]

EXPERIMENTAL SECTION

All chemicals were reagent grade and purchased from commercial sources. All reactions were carried out under a dry argon atmosphere using Schlenk techniques and vacuum line systems unless otherwise specified. Solvents were dried, distilled, and degassed prior to use. The 5,10,15,20-tetrakis(4′-hydoxylphenyl)porphyrin (**1**) was synthesized as described previously.[25]

***meso*-5,10,15,20-Tetrakis[4-((ethoxycarbonyl)methoxy)-phenyl]porphyrin (2).** Compound **1** (0.68 g, 1.0 mmol), K_2CO_3 (1.4 g, 10 mmol), ethyl bromoacetate (1.0 g, 6.0 mmol), and 18-crown-6 (53 mg, 0.2 mmol) were dissolved in 30 mL of dry acetone and stirred at room temperature for 1 day. Then the mixture was filtered, and the filtrate was evaporated to generate the crude residue, which was purified by chromatography on a silica gel column using ethyl acetate/petroleum ether (v/v = 1: 2) as eluent to give a purple solid. Yield: 87% (0.89 g). ESI-MS (CH_2Cl_2): *m*/*z* 1023.6 ($[M + H]^+$). ^1H NMR ($CDCl_3$, 400 MHz, TMS, ppm): δ −2.74 (s, 2H), 1.45 (t, *J* = 7.28 Hz, 12H), 4.45 (m, 8H), 4.94 (s, 8H), 7.32 (d, *J* = 6.88 Hz, 8H), 8.15 (d, *J* = 6.86 Hz, 8H), 8.88 (s, 8H). ^{13}C NMR ($CDCl_3$, 400 MHz, ppm): δ 14.30, 61.56, 65.80, 112.99, 114.21, 119.51, 132.02, 135.59, 157.78, 169.06.

***meso*-5,10,15,20-Tetrakis[4-((ethoxycarbonyl)methoxy)-phenyl]porphyrinatozinc(II) (3).** A mixture of **2** (0.75 g, 0.73 mmol) and $Zn(OAc)_2{\cdot}2H_2O$ (0.22 g, 1.0 mmol) in $CHCl_3$ (30 mL) was refluxed in argon atmosphere for 4 h. After cooling, the reaction mixture was washed with water for three times. The organic layer was dried over Na_2SO_4 and concentrated. The product was purified by chromatography on a silica gel column using CH_2Cl_2/CH_3OH (100:1) as eluent to give a purple solid. Yield: 93% (0.74 g). ESI-MS (CH_2Cl_2): *m*/*z* 1085.5 ($[M + H]^+$). ^1H NMR ($CDCl_3$, 400 MHz, TMS, ppm): δ1.43 (t, *J* = 7.50 Hz, 12H), 4.42 (m, 8H), 4.91 (s, 8H), 7.31 (d, *J* = 8.76 Hz, 8H), 8.15 (d, *J* = 8.13 Hz, 8H), 8.98 (s, 8H). ^{13}C NMR ($CDCl_3$, 400 MHz, ppm): δ 14.29, 60.37, 65.81, 112.86, 120.52, 131.94, 135.40, 136.27, 150.45, 157.62, 169.09.

Porphyrin 4. Compound **3** (0.54 g, 0.5 mmol) and tris-(2-aminoethyl)amine (0.73 g, 5.0 mmol) were refluxed in 40 mL of ethanol for 2 days in argon atmosphere. The solvent was evaporated, and the solid residua was washed with H_2O for five times. The water-insoluble solid was dried in vacuum to give a deep green solid (0.46 g). It was used in the next step without further purification.

Porphyrin 5. A mixture of **4** (0.46 g) and bromoacetic acid ethyl ester (1.16 g, 6.0 mmol) in 30 mL of CH_3CN was stirred in the presence of $NaHCO_3$ (0.76 g, 9 mmol) at 50 °C for 2 days in argon atmosphere. The mixture was then filtered, and the filtrate was evaporated. The residua was purified by column chromatography on silica gel (CH_2Cl_2/CH_3OH = 10: 1). The product was obtained as a purple solid by removal of the solvent. Yield: 13% (0.22 g, calculated from compound **3**). ESI-MS (CH_2Cl_2): *m*/*z* 3313.0 ($[M + H]^+$), 1657.4 ($[M + 2H]^+$). ^1H NMR ($CDCl_3$, 400 MHz, TMS, ppm): δ 1.47 (S, 143H), 2.60–3.70 (m, 85H),

dx.doi.org/10.1021/ic500238s | Inorg. Chem. 2014, 53, 4184–4191

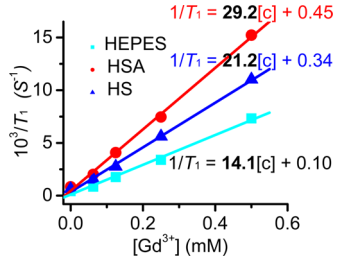

Figure 1. Linear relationship between $1/T_1$ and the concentrations of Gd(III) in 100 mM HEPES solution (■, pH = 7.2), 100 mM HEPES solution with 0.6 mM HSA (●), and HS (human blood serum, ▲).

4.79 (m, 8H), 7.35 (d, J = 8.50 Hz, 8H), 8.15 (d, J = 8.63 Hz, 1H), 8.97 (s, 8H). ^{13}C NMR ($CDCl_3$, 400 MHz, ppm): δ 28.21, 29.73, 52.06, 52.71, 55.43, 56.13, 67.83, 80.97, 81.61, 113.08, 131.91, 135.51, 150.43, 157.45, 170.21, 170.69.

TPP(H_4DTTA)$_4$. To a CH_2Cl_2 (5 mL) solution of **5** (0.17 g, 0.05 mmol) was added trifluoroacetic acid (5 mL). After stirring at ambient temperature for 1 day, the solution was evaporated and the residue redissolved in CH_3OH. To the solution was added dropwise cold diethyl ether to precipitate the product as a green solid, which was filtered and dried in vacuo. Yield: 90% (0.11 g). ESI-MS (DMSO): m/z 2375.0 ($[M + Na]^+$). ^{1}H NMR (d_6-DMSO, 400 MHz, TMS, ppm): δ −2.89 (S, 2H), 2.6−3.8 (m, 81H), 4.80 (s, 8H), 7.43 (s, 8H), 8.14 (s, 8H), 8.85 (s, 8H). ^{13}C NMR (D-DMSO, 400 MHz, ppm): δ 38.58, 52.46, 56.05, 60.22, 68.73, 108.44, 113.21, 120.71, 136.60, 138.85, 142.57, 157.53, 161.45, 169.91, 171.08.

Complex 6. To an aqueous solution of TPP(H_4DTTA)$_4$ (82 mg, 0.04 mmol) was added dropwise 1 M NaOH solution until pH = 7.0. An aqueous solution of $GdCl_3{\cdot}6H_2O$ (0.06 g, 0.16 mmol) was slowly added. To maintain the pH at 7.0, 1 M NaOH solution was further added. Upon stirring at room temperature for 1 day, an amount of cold acetone was added carefully to precipitate the product as a white solid. Yield: 92% (0.12 g). ESI-MS (CH_3OH): m/z 3020.3 ($[M + 3H_2O]^-$). Anal. Calcd for $C_{108}H_{134}Gd_4N_{20}Na_4O_{48}$ (Na_4TPP-(DTTAGd)$_4{\cdot}8H_2O$): C, 40.52; H, 4.22; N, 8.75; Gd 19.65. Found: C, 40.82; H, 4.38; N, 8.58; Gd 19.87.

Physical Measurements. ^{1}H and ^{13}C NMR spectra were recorded at 400 MHz on a Bruker Avance III NMR spectrometer. Gadolinium content was determined on an Ultima 2 inductively coupled plasma OES (ICP-OES) spectrophotometer. Elemental analyses (C, H, and N) were carried out on a Perkin-Elemer model 240C elemental analyzer. Electrospray ionization mass spectra (ESI-MS) were performed on a Finnigan LCQ mass spectrometer. Emission and excitation spectra were recorded on a Perkin-Elmer LS55 luminescence spectrometer with a red-sensitive photomultiplier type R928. UV−vis absorption spectra were measured on a Perkin-Elmer Lambda 25 UV−vis spectrometer. Emission lifetime was determined on an Edinburgh analytical instrument (FLS920 fluorescence spectrometer) using picosecond pulsed diode lasers of the EPL at 375 nm excitation. The absolute emission quantum yields (Φ_{em}) at room temperature were recorded on an Edinburgh analytical instrument (FLS920 fluorescence spectrometer) with integrating sphere. All of the spectra were recorded at 25 °C in a 100 mM HEPES buffer solution at pH = 7.2.

T_1 Measurements. The longitudinal relaxation times (T_1) of complex **6** were measured by a standard inversion−recovery pulse sequence on a PQ-001 NMR Analyzing & Imaging system (Shanghai Niumag Corp.) at 0.55 T and 25 °C. In each case, five samples were prepared separately, in which the concentrations of Gd(III) were 0, 0.0625, 0.125, 0.25, and 0.5 mM in 100 mM HEPES buffer solutions at pH = 7.2. The concentration of Gd(III) was detected by ICP-OES. The relaxivity r_1 is commonly used to express the ability of proton relaxation enhancement of a paramagnetic compound. It is defined as the slope of eq 1 with mM^{-1} s^{-1} as units

$$(1/T_1)_{obs} = (1/T_1)_d + r_1[M] \quad (1)$$

where $(1/T_1)_{obs}$ and $(1/T_1)_d$ are the observed values in the presence and absence of the paramagnetic species and [M] is the concentration of the paramagnetic species.

T_1-Weighted MRI Phantom Images. Phantom images were performed using a MiniMR-60 NMR Analyzing & Imaging system (Shanghai Niumag Corp.). Instrumental parameters were set as follows: a 0.55 T magnet, section thickness = 5.0 mm, TE = 20 ms, TR = 200 ms.

Fluorescent Displacement Experiments. Warfarin and dansylglycine are well-known probes for site I and site II, respectively.[26] Free warfarin and dansylglycine exhibit weak fluorescence emissions. Upon binding to HSA, their fluorescence emissions centered at 380 and 490 nm were greatly enhanced. If the binding of the probes to HSA was displaced by other species, the fluorescence of the probes will be remarkably decreased. To 100 mM HEPES buffer solutions (pH = 7.2) containing 5 μM of the fluorescent probe and HSA were added 40, 20, 10, 5, 2.5, 1.25, 0.625, and 0 μM of complex **6**. Emission

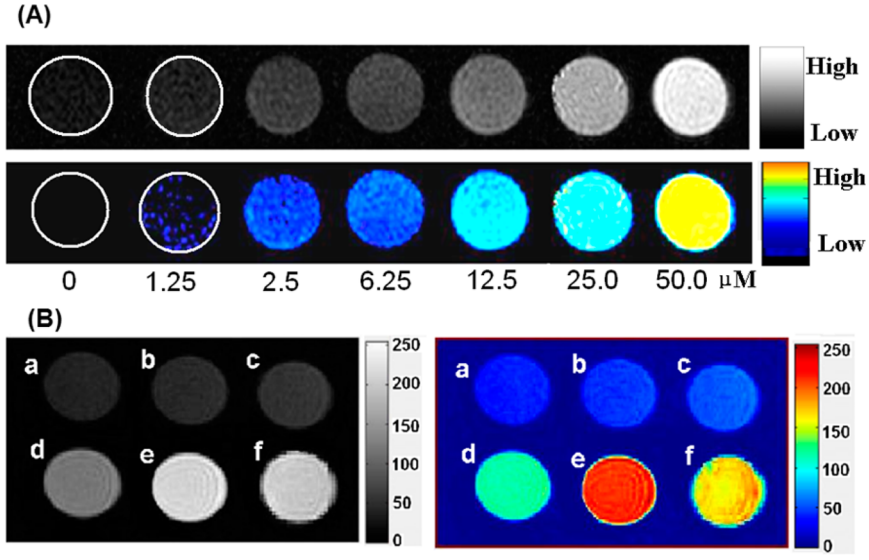

Figure 2. (A) T_1-weighted phantom MR images for complex **6** with a concentration of 0−50.0 μM. (B) T_1-weighted phantom MR images for complex **6**. (a) 100 mM HEPES buffer solution (pH = 7.2); (b) 100 mM HEPES buffer solution with 0.6 mM HSA; (c) HS; (d) 31.25 μM complex **6** in 100 mM HEPES solution; (e) 31.25 μM complex **6** in 100 mM HEPES solution with 0.6 mM HSA; (f) 31.25 μM complex **6** in HS.

dx.doi.org/10.1021/ic500238s | Inorg. Chem. 2014, 53, 4184−4191

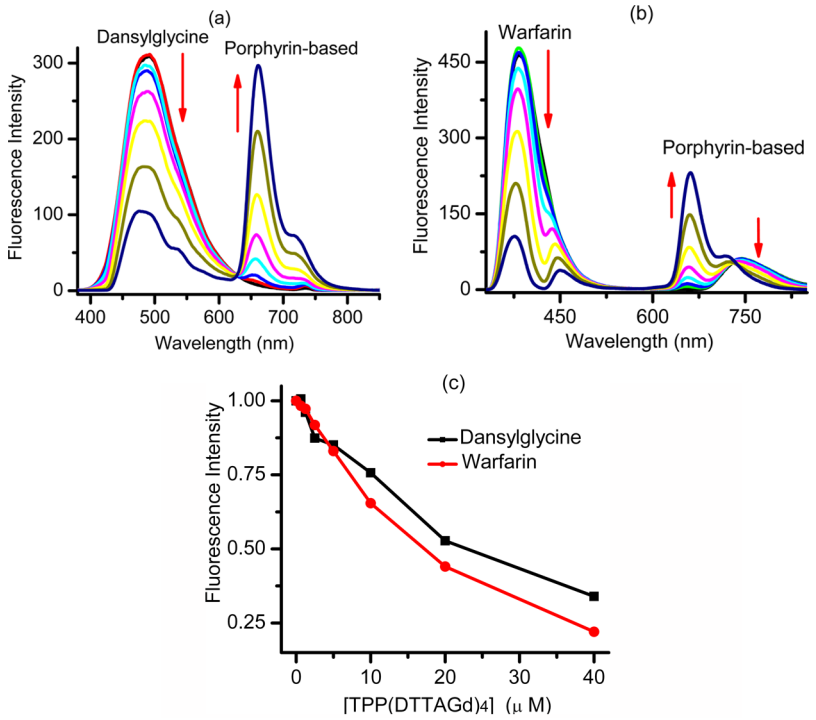

Figure 3. (a) Fluorescence spectral changes of HSA binding dansylglycine (1:1) upon displacement by complex **6**. (b) Fluorescence spectral changes of HSA binding warfarin (1:1) upon displacement by complex **6**. (c) Fluorescence intensity changes of HSA binding dansylglycine/warfarin (1:1) at 380 (warfarin) or 490 nm (dansylglycine) upon gradual addition of complex **6**.

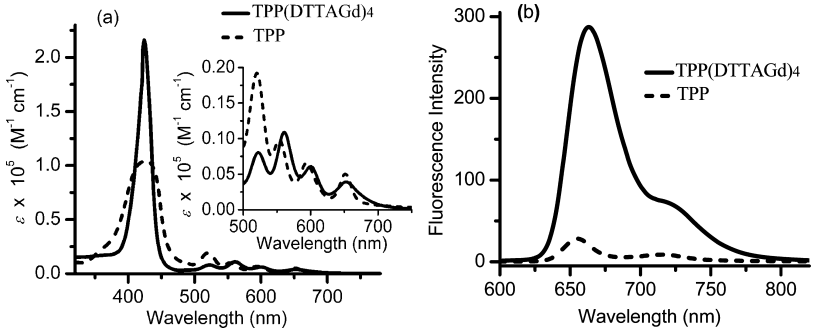

Figure 4. (a) Absorption spectra of 5 μM complex **6** in HEPES buffer solution (solid line) and 5 μM TPP in DMSO/water (1%) (dashed line). (b) Fluorescence spectra of 20 μM complex **6** in HEPES buffer solution (solid line) and 20 μM TPP in DMSO/water (1%) (dashed line) excited at 441 nm.

spectra of the eight samples were measured at 25 °C. Excitation and emission wavelengths used for dansylglycine were 365 and 490 nm, and those for warfarin were 320 and 380 nm.

Singlet Oxygen Detection by ADPA. Generation of singlet oxygen was detected chemically according to the literature using the disodium salt of 9,10-anthracenedipropionic acid (ADPA, Sigma) as a singlet oxygen sensor.[5,27,28] ADPA is bleached by singlet oxygen to its corresponding endoperoxide (Figure 6). The reaction was monitored spectrophotometrically by recording the decrease in optical density at 378 nm. A D_2O solution of 10 μM complex **6** and 300 μM of ADPA were used to measure the UV−vis absorption spectra. 5,10,15,20-Tetraphenylporphyrin (10 μM) and ADPA (300 μM) dispersed in D_2O solution containing 1% DMSO were used as control samples. Solutions were saturated with oxygen and exposed to 650 ± 20 or 475−720 nm light irradiation, and their optical densities at 378 nm were recorded every 10 or 2 min in a UV−vis spectrophotometer. The light source was obtained from a 500 W tungsten lamp with 650 ± 20 nm narrow-band or 475−720 nm wide-band filters.

After being saturated with oxygen and irradiated with 650 ± 20 nm band irradiation, fluorescence spectra of a D_2O solution containing 5 μM complex **6** and 25 μM of ADPA were also recorded every 5 min.

Table 1. Spectral Properties of Complex 6

λ_{ex} (nm)	393	441	522	561	610
Φ (%)	5.45	5.28	4.28	5.33	7.52
ε (M^{-1} cm^{-1})	30 551	52 025	8077	10 900	4553
brightness[a] (mM^{-1} cm^{-1})	1.67	2.75	0.35	0.58	0.34
lifetime[b]			8.54 ns		

[a]Brightness determined as the product of extinction coefficient ε and quantum yield Φ.[24] [b]Lifetime was measured upon excitation at 375 nm.

A D_2O solution of 5 μM TPP and 25 μM ADPA containing 1% DMSO were used as control samples.

Singlet Oxygen Detection by 2,5-Dimethylfuran. 2,5-Dimethylfuran was also used to detect generation of singlet oxygen.[29] In the presence of singlet oxygen, 2,5-dimethylfuran undergoes a [4 + 2] cycloaddition reaction to give an ozonide, which dimerizes to give a peroxide product as a single diastereomer (Figure 7). Photooxidation of 2,5-dimethylfuran was accomplished through 650 ± 20 nm light irradiation. Complex **6** (9.0 mg, 3.0 μmol) and 2,5-dimethylfuran (0.5 μL, 0.45 mmol) were dissolved in 1.0 mL of d_6-DMSO.

dx.doi.org/10.1021/ic500238s | Inorg. Chem. 2014, 53, 4184−4191

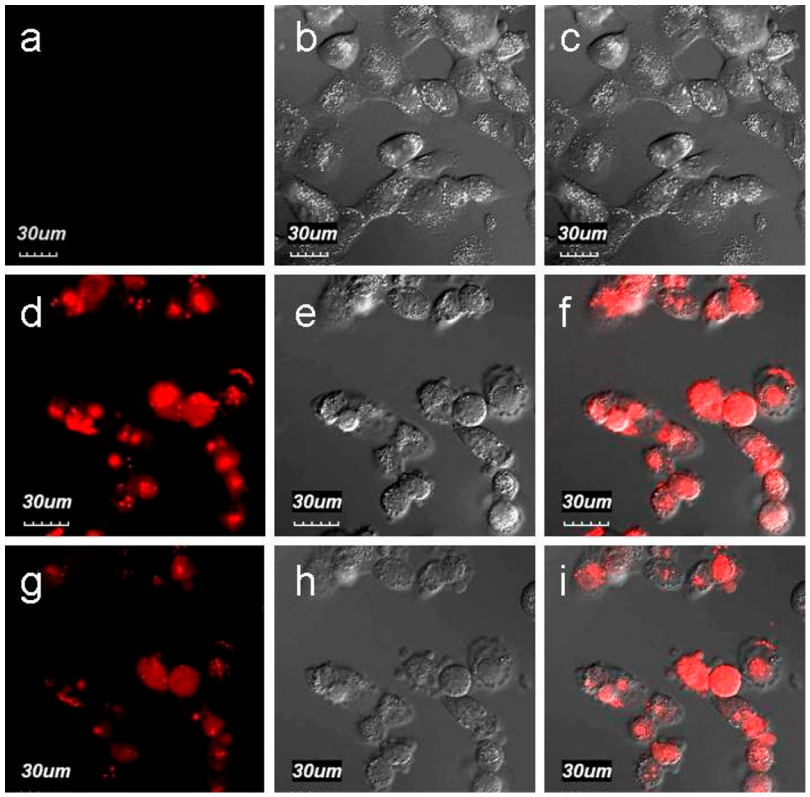

Figure 5. Confocal fluorescence images in human lung cancer cells H1299. (a) Cells without being incubated with complex **6**. (b) Bright-field image of a. (c) Overlay image of a and b. (d) Cells incubated with 20 μM complex **6** in PBS buffer for 4 h (excited by a 405 nm laser). (e) Bright-field image of d. (f) Overlay image of d and e. (g) Same sample as d but excited by a 568 nm laser source. (h) Bright-field image of g. (i) Overlay image of g and h.

Upon saturation with oxygen, the solution was irradiated and the photo-oxidation progress was monitored using NMR spectroscopy.

Fluorescence Imaging Experiment. A human lung cancer cell line H1299 was purchased from commercial sources. Cells were grown in MEM (Modified Eagle's Medium) supplemented with 10% FBS (Fetal Bovine Serum) at 37 °C and 5% CO_2. Cells (5×10^8 /L) were plated on 18 mm glass coverslips and allowed to adhere for 24 h. Cells were mounted for direct microscopic observation at 37 °C. Confocal fluorescence images of cells were performed with an Olympus Fluo View FV1000 laser-scanning microscope. A 60× oil-immersion objective lens was used. Excitation was carried out with a semiconductor laser at λ = 405 or 568 nm, and emission was collected in the range λ = 600−700 nm, including the maximum emission of complex **6** at 665 nm. Lung cancer cells H1299 were incubated with a PBS solution of complex **6** (20 μM) for dye loading for 4 h at 37 °C. Stained cells were washed three times with PBS buffer. Then the treated cells were imaged by fluorescence microscopy. For the control experiment, cells were washed three times with PBS buffer and then imaged by fluorescence microscopy directly.

RESULTS AND DISCUSSION

The ligand was synthesized by a five-step route as shown in Scheme 2. The initial step was nucleophilic substitution of 5,10,15,20-tetrakis(4′-hydoxylphenyl)porphyrin (**1**) with four ethyl bromoacetates in a yield of 87%. Porphyrin **2** was stabilized by coordination of Zn^{2+} to give Zn(II) complex **3** in 93% yield. Because of the poor stability of Zn(II) porphyrin complex in hot solution and long-term reaction process, the overall yield of the following two-step amination and carboxymethylation was only 13%. Free ligand TPP(H_4DTTA)$_4$ was then obtained from an ester hydrolysis reaction in 90% yield in which coordinated Zn^{2+} was lost during the hydrolysis process in the presence of trifluoroacetic acid. Complex **6** was prepared by mixing the free ligand with $GdCl_3 \cdot 6H_2O$ in a 1:4 molar ratio at pH = 7.0 and characterized by ESI-MS and elemental analysis.

T_1 Relaxivity and in Vitro MR Imaging. The relaxivity of complex **6** was as high as 14.1 mM^{-1} s^{-1} per Gd(III) in 100 mM HEPES buffer solution (25 °C, pH = 7.2, 23 MHz). Investigated in a buffer solution with 0.6 mM HSA, the relaxivity of complex **6** was further increased from 14.1 to 29.2 mM^{-1} s^{-1} (25 °C, pH = 7.2, 23 MHz) with 107% enhancement (Figure 1). The signal intensity of T_1-weighted phantom MR image was distinctly improved with the increase of the concentrations of complex **6** (Figure 2A). In addition, the signal intensity of T_1-weighted phantom MR image was significantly improved (Figure 2B, e) upon binding to HSA. Quite high relaxivity (14.1 mM^{-1} s^{-1} for per Gd(III)) is ascribed to the large molecular weight (fw = 3201) and high molecular rigidity, thus inducing a long rotational tumbling time (τ_R).[9] In addition, the HSA binding further enhanced the molecular weight of complex **6** that induces a surprising increase of relaxivity.

To investigate the relaxivity of complex **6** under physiological condition, relaxivity measurements were also performed in human blood serum (HS) (Figure 1). Remarkably, the relaxivity of complex **6** was estimated as high as 21.2 mM^{-1} s^{-1} (32 °C, 23 MHz) when it was measured in HS. The signal intensity of the T_1-weighted phantom MR image in HS (Figure 2B, f) was much improved relative to that in HEPES buffer (Figure 2B, d).

Interaction between Complex 6 and HSA. There are a variety of biomacromolecules in the human body such as protein, glycogen, and nucleic acid, etc. It is likely that the interaction of contrast agents with macromolecules could slow down the

dx.doi.org/10.1021/ic500238s | Inorg. Chem. 2014, 53, 4184−4191

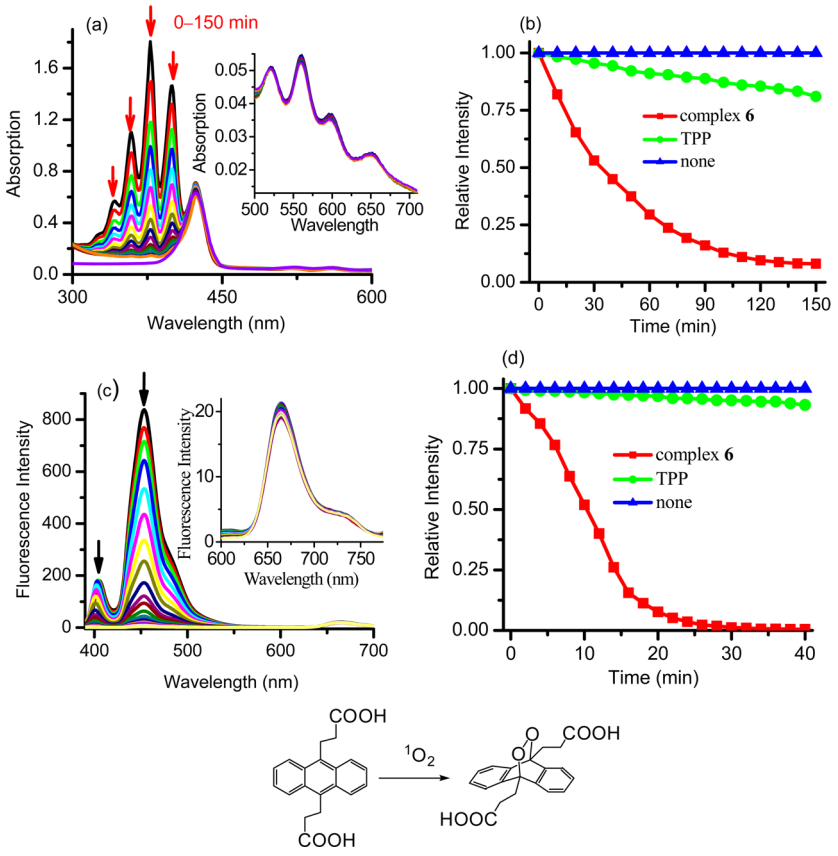

Figure 6. (a) Time-dependent bleaching of ADPA by singlet oxygen generated from complex **6**. (b) Change in the absorption of ADPA at 378 nm with exposure time. (c) Time-dependent fluorescence quenching of ADPA by singlet oxygen generated from complex **6**. (d) Change in emission intensity of ADPA at 453 nm with exposure time. Solutions were exposed to far-red light irradiation at 650 ± 20 nm.

tumbling rate and increase the relaxivity of Gd-based contrast agents. HSA is the most abundant protein in blood plasma and cerebral spinal fluid with a molecular weight of 66 kDa and a concentration between 0.53 and 0.75 mM.[19,26] It is known that HSA can accumulate in a tumor since it is taken up by tumor cells at a higher level relative to normal cells.[19] Upon binding to HSA, the relaxivity of complex **6** is remarkably enhanced from 14.1 to 29.2 mM^{-1} s^{-1} and the signal intensity of the T_1-weighted phantom MR image was also significantly improved. Although the emission spectrum of complex **6** was little shifted (from 665 to 661 nm), the emission intensity exhibited 26% enhancement. The noncovalent interaction of HSA with complex **6** originates mostly from electrostatic interaction because the inner surface of the hydrophobic pocket of HSA is positively charged whereas complex **6** dispalys four negative charge. Hydrophobicity and stereospecificity are likely another two factors that result in the interaction of HSA with complex **6**.[19] Such noncovalent interactions are of particular significance because they may afford better accessibility toward low concentration target with less toxicity and longer half-life of metabolism in the human body.[9]

To determine whether complex **6** binds at Suddlow site I (subdomain IIA) or Suddlow site II (subdomain IIIA) of HSA, displacement experiments were performed using warfarin as a fluorescent probe for site I and dansylglycine for site II.[26] Although free warfarin or dansylglycine exhibits weak fluorescence, the emission centered at 380 (warfarin) or 490 nm (dansylglycine) is greatly enhanced upon binding to HSA. When the binding site of warfarin or dansylglycine to HSA is displaced by other species, the fluorescence will be remarkably reduced. As shown in Figure 3, the fluorescence of both warfarin and dansylglycine was gradually reduced by addition of complex **6**, implying that complex **6** binds to HSA at both site I and site II.

Spectral Properties of Complex 6. The TPP moiety is an intense chromophore with strong Soret band and medium Q-band absorption. As shown in Figure 4a, relative to free TPP, the Q-band of complex **6** shows a little red shift due to the more extended system upon incorporating TPP with four Gd–DTTA units. This wide range of visible absorption qualifies complex **6** as a efficient photosensitizer. Upon excitation at λ_{ex} > 350 nm, complex **6** shows intense emission at 665 nm, which is a little red shifted with a much stronger intensity relative to that of free TPP (655 nm, Figure 4b). The emission of complex **6** can be excited by a wide range of exciting wavelengths. Upon excitation at different wavelengths, the fluorescence quantum yield of complex **6** was estimated as 4.3–7.5% (Table 1). Upon irradiation by a red light at 610 nm, far-red luminescence occurred with the maximum at 665 nm and Φ_{em} = 7.5%. The far-red emission triggered by red excitation ensures complex **6** as an optimal probe that is available for deep tissue imaging and whole-body imaging.[24] Additionally, the fluorescence spectrum was obviously dependent on pH value. The emission at 665 nm progressively enhanced with the increase of pH, and there existed a jump from pH = 5.5 to 6.5 (Figure S3, Supporting Information). The solution changed from green to purple with the increase of pH from 3.0 to 10.0.

dx.doi.org/10.1021/ic500238s | Inorg. Chem. 2014, 53, 4184–4191

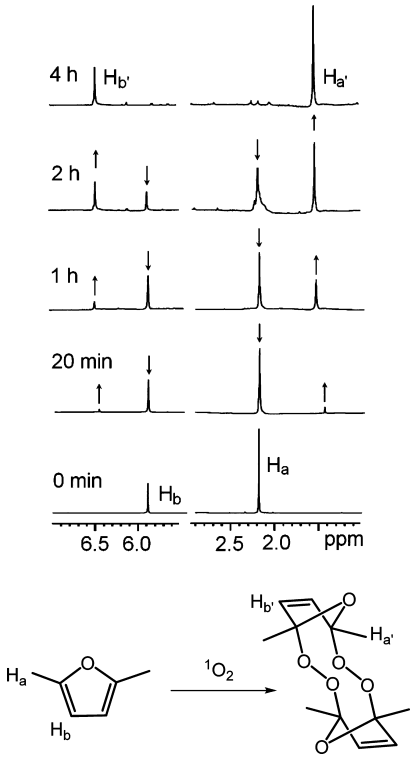

Figure 7. Process of photo-oxidation of 2,5-dimethylfuran by singlet oxygen generated from complex **6**, monitored using ^{1}H NMR spectroscopy. Solutions were exposed to far-red light irradiation at 650 ± 20 nm.

Fluorescence Imaging. As both photosensitizer and luminophore, the central TPP moiety generates effectively singlet-oxygen upon excitation with a far-red irradiation (650 nm). Furthermore, the TPP moiety exhibits a far-red emission (665 nm) with favorable luminescence efficiency. The superior far-red excitation and emission ensure complex **6** applicable to PDT and PDD in deep tissue.[5,24]

Human lung cancer cell H1299 was used to verify the cellular uptake of complex **6** (Figure 5). Confocal fluorescence image experiments upon irradiation with a 405 (Figure 5d–f) or 568 (Figure 5g–i) nm laser revealed that red fluorescence of complex **6** was distributed in the whole inside space of cells, which was clearly naked-eye observable (Figure 5d or 5g). Bright-field measurements (Figure 5e or 5h) indicated that the cells were viable throughout the imaging experiments upon treatment with complex **6**. It is ingested harmlessly by living cells with sufficiently low cytotoxicity so as to be applied in vivo.

Photodynamic Activity of Complex 6. Generation of singlet oxygen triggered by complex **6** was detected chemically using the disodium salt of 9,10-anthracenedipropionic acid (ADPA) as a detector (Figure 6), which is bleached to nonfluorescent endoperoxide in the presence of $^1O_2$.[5,27] Figure 6b shows the decrease of the absorption at 378 nm as a function of irradiation time. The sharp decrease in the absorbance of ADPA with irradiation time demonstrated the generation of $^1O_2$ when a D_2O solution of complex **6** was exposed to light irradiation at 650 ± 20 nm. The absorbance of ADPA at 378 nm decreased much more slowly in the case of free TPP (decreased about 20% in 150 min), indicating that free TPP exhibits a much lower efficiency to generate $^1O_2$ than complex **6**. Incorporating tetraphenylporphyrin with four Gd–DTTA moieties thus improves significantly the capability to generate $^1O_2$ due to the much increased water solubility. In striking contrast, distinct variation in the absorption of ADPA at 378 nm was unobserved in the corresponding D_2O solution without porphyrin species under light irradiation (Figure 6b), further confirming that the bleaching of ADPA in the presence of porphyrin is induced by singlet oxygen and not by the irradiated light. Upon excitation at 370 nm, ADPA exhibits intense fluorescence at 453 nm. As depicted in Figure 6c/6d, this fluorescence band was progressively reduced due to formation of nonfluorescent endoperoxide through oxidation of ADPA by singlet oxygen that is generated upon exposing complex **6** to visible irradiation. In contrast, the absorption (Figure 6a, inner) and fluorescence (Figure 6c, inner) of complex **6** itself was almost unchanged upon exposure to visible irradiation, implying that it exhibits excellent photostability.

Generation of $^1O_2$ was further confirmed by a chemical trapping method using 2,5-dimethylfuran as a substrate, which underwent a [4 + 2] cycloaddition reaction with singlet oxygen and then dimerized rapidly to a peroxide product.[29] The photo-oxidation process of 2,5-dimethylfuran was monitored by ^{1}H NMR spectroscopy. As shown in Figure 7, the ^{1}H NMR spectrum of 2,5-dimethylfuran exhibits two singlet peaks at 5.90 (2H, furan) and 2.19 ppm (6H, methyl). When a d_6-DMSO solution of 2,5-dimethylfuran was exposed to red light (650 ± 20 nm) irradiation in the presence of 1/150 equiv of complex **6**, the signals at 5.90 and 2.19 ppm decreased gradually and vanished entirely in 4 h. Meanwhile, a group of new signal peaks occurred at 6.47 and 1.55 ppm and enhanced progressively due to conversion of 2,5-dimethylfuran to the peroxide product. Thus, the photo-oxidization experiment further demonstrates that singlet oxygen is indeed generated upon irradiation of complex **6** with visible light.

■ CONCLUSION

Complex **6** with four Gd–DTTA moieties appended to a porphyrin framework was elaborately designed. The longitudinal relaxivity is as high as 14.1 mM^{-1} s^{-1} in HEPES buffer solution (pH = 7.2). Upon interacting with HSA, r_1 is increased to 29.2 mM^{-1} s^{-1} with 107% enhancement. Since HSA can be taken up by tumor cells at a higher level relative to normal cells, the biological compatibility and targeting are significantly enhanced upon binding to HSA, whereas the cell toxicity is much reduced. Fluorescence imaging studies indicate that it can be ingested harmlessly by living cells. The Gd(III)–porphyrin species exhibits much higher photodynamic activity than free TPP, in which singlet oxygen is efficiently generated upon exposure to far-red light irradiation at 650 ± 20 nm. It is a potential candidate as a clinical theranostic agent with excellent functions for multimodal imaging and photodynamic therapy.

■ ASSOCIATED CONTENT

Supporting Information

Figures giving additional UV–vis and emission spectra. This material is available free of charge via the Internet at http://pubs.acs.org.

■ AUTHOR INFORMATION

Corresponding Author

*E-mail: czn@fjirsm.ac.cn.

Notes

The authors declare no competing financial interest.

■ ACKNOWLEDGMENTS

We are thankful for financial support from the NSFC (20931006, 91122006, and 21390392), the 973 project (2014CB845603) from MSTC, and the NSF of Fujian Province (2011J01065).

■ REFERENCES

(1) Celli, J. P.; Spring, B. Q.; Rizvi, I.; Evans, C. L.; Samkoe, K. S.; Verma, S.; Pogue, B. W.; Hasan, T. *Chem. Rev.* **2010**, *12*, 2795−2838.
(2) (a) Huang, X.; El-Sayed, I. H.; Qian, W.; El-Sayed, M. A. *J. Am. Chem. Soc.* **2006**, *128*, 2115−2120. (b) Ho, C.-L.; Wong, K.-L.; Kong, H.-K.; Ho, Y.-M.; Chan, C. T.-L.; Kwok, W.-M.; Leung, K. S.-Y.; Tam, H.-L.; Lam, M. H.-W.; Ren, X.-F.; Ren, A.-M.; Feng, J.-K.; Wong, W.-Y. *Chem. Commun.* **2012**, *48*, 2525−2527.
(3) (a) Kelkar, S. S.; Reineke, T. M. *Bioconjugate Chem.* **2011**, *22*, 1879−1903. (b) Zhao, Z.; Chan, P. S.; Li, H.; Wong, K. L.; Wong, R. N. S.; Mak, N.-K.; Zhang, J.; Tam, H.-L; Wong, W.-Y.; Kwong, D. W. J.; Wong, W.-K. *Inorg. Chem.* **2012**, *51*, 812−821. (c) Chui, C.-H.; Wang, Q.; Chow, W.-C.; Yuen, M. C.-W.; Wong, K.-L.; Kwok, W.-M.; Cheng, G. Y.-M.; Wong, R. S.-M.; Tong, S.-W.; Chan, K.-W.; Lau, F.-Y.; Lai, P. B.-S.; Lam, K.-H.; Fabbri, E.; Tao, X.-M.; Gambari, R.; Wong, W.-Y. *Chem. Commun.* **2010**, *46*, 3538−3540.
(4) Ke, H.; Wang, J.; Dai, Z.; Jin, Y.; Qu, E.; Xing, Z.; Guo, C.; Yue, X.; Liu, J. *Angew. Chem., Int. Ed.* **2011**, *50*, 3017−3021.
(5) Liang, X.; Li, X.; Yue, X.; Dai, Z. *Angew. Chem., Int. Ed.* **2011**, *50*, 11622−11627.
(6) Nystrom, A. M.; Wooley, K. L. *Acc. Chem. Res.* **2011**, *44*, 969−978.
(7) Lee, S. M.; Song, Y.; Hong, B. J.; MacRenaris, K. W.; Mastarone, D. J.; O' Halloran, T. V.; Meade, T. J.; Nguyen, S. B. T. *Angew. Chem., Int. Ed.* **2010**, *49*, 9960−9964.
(8) Caravan, P.; Ellison, J. J.; McMurry, T. J.; Lauffer, R. B. *Chem. Rev.* **1999**, *99*, 2293−2352.
(9) Geraldes, C. F.; Laurent, S. *Contrast Media Mol. Imaging* **2009**, *4*, 1−23.
(10) (a) Wang, B.; Hai, J.; Wang, Q.; Li, T.; Yang, Z. *Angew. Chem., Int. Ed.* **2011**, *123*, 3119−3122. (b) Zhang, X. L.; Jing, X.; Liu, T.; Han, G.; Li, H. Q.; Duan, C. Y. *Inorg. Chem.* **2012**, *51*, 2325−2331.
(11) Que, E. L.; Chang, C. J. *Chem. Soc. Rev.* **2010**, *39*, 51−60.
(12) Koullourou, T.; Natrajan, L. S.; Bhavsar, H.; Simon, J. A.; Feng, J. H; Narvainen, J.; Shaw, R.; Scales, E.; Kauppinen, R.; Kenwright, A. M.; Faulkner, S. *J. Am. Chem. Soc.* **2008**, *130*, 2178−2179.
(13) Gad, F.; Zahra, T.; Francis, K. P.; Hasan, T.; Hamblin, M. R. *Photochem. Photobiol. Sci.* **2004**, *3*, 451−458.
(14) Bonnett, R. *Chem. Soc. Rev.* **1995**, *24*, 19−33.
(15) DeRosa, M. C.; Crutchley, R. J. *Coord. Chem. Rev.* **2002**, *233*−*234*, 351−371.
(16) Detty, M. R.; Gibson, S. L.; Wagner, S. J. *J. Med. Chem.* **2004**, *47*, 3897−3915.
(17) Samia, A. C. S.; Chen, X.; Burda, C. *J. Am. Chem. Soc.* **2003**, *125*, 15736−15737.
(18) Livramento, J. B.; Toth, E.; Sour, A.; Borel, A.; Merbach, A. E.; Ruloff, R. *Angew. Chem., Int. Ed.* **2005**, *44*, 1480−1484.
(19) Chan, K. W. Y.; Wong, W. T. *Coord. Chem. Rev.* **2007**, *251*, 2428−2451.
(20) Werner, E. J.; Datta, A.; Jocher, C. J.; Raymond, K. N. *Angew. Chem., Int. Ed.* **2008**, *47*, 8568−8580.
(21) Song, Y.; Kohlmeir, E. K.; Meade, T. J. *J. Am. Chem. Soc.* **2008**, *130*, 6662−6663.
(22) (a) Eggenspiller, A.; Michelin, C.; Desbois, N.; Richard, P.; Barbe, J.-M.; Denat, F.; Licona, C.; Gaiddon; Sayeh, A.; Choquet, P.; Gros, C. P. *Eur. J. Org. Chem.* **2013**, 6629−6643. (b) Gros, C. P.; Eggenspiller, A.; Nonat, A.; Barbe, J.-M.; Denat, F. *Med. Chem. Commun.* **2011**, *2*, 119−125. (c) Song, Y.; Zong, H.; Trivedi, E. R.; Vesper, B. J.; Waters, E. A.; Barrett, A. G. M.; Radosevich, J. A.; Hoffman, B. M.; Meade, T. J. *Bioconjugate Chem.* **2010**, *21*, 2267−2275. (d) Goswami, L. N.; White, W. H.; Spernyak, J. A.; Ethirajan, M.; Chen, Y.; Missert, J. R.; Morgan, J.; Mazurchuk, R.; Pandey, R. K. *Bioconjugate Chem.* **2010**, *21*, 816−827. (e) Hindre, F.; Le Plouzennec, M.; De Certaines, J. D.; Foultier, M. T.; Patrice, T.; Simonneaux, G. *J. Magn. Reson. Imaging* **1993**, *3*, 59−65.
(23) Avedano, S.; Tei, L.; Lombardi, A.; Giovenzana, G. B.; Aime, S.; Longo, D.; Botta, M. *Chem. Commun.* **2007**, 4726−4728.
(24) Shcherbakova, D. M.; Subach, O. M.; Verkhusha, V. V. *Angew. Chem., Int. Ed.* **2012**, *51*, 10724−10738.
(25) Esch, J. H.; Feiters, M. C.; Peters, A. M.; Nolte, R. J. M. *J. Phys. Chem.* **1994**, *98*, 5541−5551.
(26) Esqueda, A. C.; Lopez, J. A.; Andreu-de-Riquer, G.; Alvarado-Monzon, J. C.; Ratnakar, J.; Lubag, A. J. M.; Sherry, A. D.; De Leon-Rodrıguez, L. M. *J. Am. Chem. Soc.* **2009**, *131*, 11387−11391.
(27) Roy, I.; Ohulchanskyy, T. Y.; Pudavar, H. E.; Bergey, J. E.; Oseroff, A. R.; Morgan, J.; Dougherty, T. J.; Prasad, P. N. *J. Am. Chem. Soc.* **2003**, *125*, 7860−7865.
(28) Lindig, B. A.; Rodgers, M. A. J.; Schaap, A. P. *J. Am. Chem. Soc.* **1980**, *102*, 5590−5593.
(29) Oar, M. A.; Dichtel, W. R.; Serin, J. M.; Frechet, J. M. *Chem. Mater.* **2006**, *18*, 3682−3692.

■ NOTE ADDED AFTER ASAP PUBLICATION

This paper was published ASAP on April 2, 2014. Reference 22 was changed. The revised paper was reposted on April 9, 2014.